decomposed to give 1,1,1,3,3,3-hexafluoro-2-[(phenylthio)-methyl]-2-propanol (**8**)[9] in almost quantitative yield upon prolonged exposure to air. On the other hand, similar treatment of the benzaldehyde adduct *erythro*-**4b**[5] with KH gave a signal at δ_{Sn} -239.52 at -30 °C, suggesting the formation of 1,2-oxastannetanide **5b**. When **5b** was heated without isolation (50 °C, THF, 5 h), (*Z*)-phenyl β-styryl sulfide (**6b**) was exclusively obtained in 82% yield, showing that the olefin formation proceeds in the same manner as that using *erythro*-**4b** itself although the reaction conditions are much milder.[10]

Product **5a** was recrystallized from dichloromethane–hexane to afford colorless needles, which melted at 125–130 °C with decomposition.[11] The X-ray crystallographic analysis of **5a** indicated that it has a very distorted TBP (trigonal bipyramid) structure (Figure 1).[12] This is the first example of an anionic pentacoordinate tin compound with a four-membered ring.[13] Oxygen and one phenyl group on the stannetanide occupy apical positions. The bond angle O(1)–Sn(1)–C(19) between two apical bonds deviates by 14.9(2)° from 180°. The bond length of Sn-(1)–O(1) [2.401(5) Å] is longer than that of Sn–O(ax) [2.276(7) Å] reported for compound **9**.[14] The axial bond Sn(1)–C(19) [2.188(8) Å] is longer than exocyclic equatorial bonds Sn(1)–C(7) [2.140(7) Å] and Sn(1)–C(13) [2.136(8) Å], but is slightly shorter than the endocyclic Sn(1)–C(25) bond [2.200(7) Å].

The most outstanding structural feature is that the Sn atom is not on the plane of three equatorial ligands [C(7), C(13), and C(25)], but is located 0.442 Å above it. On the other hand, the four-membered ring is approximately coplanar, being one of the common features for pentacoordinate compounds such as **1** and **2**. The strain of the four-membered ring seems to be reduced by elongating the apical Sn–O(1) bond and making the angle O-(1)–Sn–C(25) acute.

Acknowledgment. This work was partially supported by a Grant-in-Aid for Scientific Research on Priority Area of Organic Unusual Valency No. 04217205 (T.K.) and a Grant-in-Aid for Scientific Research (A) No. 04403005 (R.O.) from the Ministry of Education, Science, and Culture, Japan. We are grateful to Dr. N. Tokitoh of The University of Tokyo for the determination of the X-ray structure of **5a**. We also thank Central Glass and Tosoh Akzo Co. Ltd. for gifts of hexafluoroacetone trihydrate and alkyllithiums, respectively.

Supplementary Material Available: X-ray crystallographic data with tables of thermal and positional parameters, bond lengths, and bond angles for **5a** (14 pages). Ordering information is given on any current masthead page.

(9) Boeré, R. T.; Willis, C. J. *Can. J. Chem.* **1985**, *63*, 3530.

(10) Heating *erythro*-**4b** (110 °C, toluene, 45 min) afforded (*Z*)-**6b** in 89.7% yield (see ref 5).

(11) **5a**: colorless crystals; mp 125–130 °C (dec) (CH_2Cl_2–hexane); ^{1}H NMR (CD_3CN) δ 3.56 [s, 24 H, (OCH_2CH_2)$_6$], 5.05 (s, 1 H, $^2J_{HSn}$ = 98 Hz, C*H*S), 7.03–7.25 (m, 14 H, SC_6H_5 and *m*- and *p*-H of $SnPh_3$), 7.72 (dd, $^4J_{HH}$ = 2 Hz, $^3J_{HH}$ = 7 Hz, 6 H, *o*-H of $SnPh_3$); ^{13}C NMR (CD_3CN) δ 55.78 ($^1J_{CSn}$ = 462 Hz, Sn*C*H), 70.24 (OCH_2CH_2), 80.71 [sept, $^2J_{CF}$ = 25 Hz, $C(CF_3)_2$], 125.12, 126.49 [q, $^1J_{CF}$ = 292 Hz, $C(CF_3)(C'F_3)$], 127.38, 127.42, 127.57 ($^2J_{CSn}$ = 50 Hz, *o*-C of SnPh), 127.65 [q, $^1J_{CF}$ = 291 Hz, $C(CF_3)(C'F_3)$], 128.80 ($^3J_{CSn}$ = 70 Hz, *m*-C of SnPh), 137.87 ($^4J_{CSn}$ = 38 Hz, *p*-C of SnPh), 141.83 ($^3J_{CSn}$ = 55 Hz, *ipso*-C of SPh), 148.87 ($^1J_{CSn}$ = 525 Hz, *ipso*-C of SnPh); ^{19}F NMR ($CDCl_3$) δ -75.09 (q, $^4J_{FF}$ = 8.8 Hz, 3 F) and -71.77 (q, $^4J_{FF}$ = 8.8 Hz, 3 F); ^{119}Sn NMR (THF) δ -229.65. Anal. Calcd for $C_{40}H_{45}F_6KO_7SSn\cdot H_2O$: C, 50.06; H, 4.73. Found: C, 50.14; H, 4.70.

(12) $C_{40}H_{45}F_6KO_7SSn\cdot CH_2Cl_2\cdot H_2O$, FW = 1044.58, crystal dimensions (mm) 0.500 × 0.250 × 0.250, triclinic, space group $P\bar{1}$, a = 13.789(2) Å, b = 14.522(2) Å, c = 12.550(3) Å, α = 92.46(2)°, β = 95.25(2)°, γ = 69.93(1)°, V = 2350.5(7) Å^3, Z = 2, D_{calcd} = 1.476 g/cm^3, R = 0.054 (R_w = 0.053). Full details of the crystallographic structure analysis are described in the supplmentary material.

(13) For pentacoordinate tin complexes by intramolecular coordination, see: Harrison, P. G.; Lambert, K.; King, T. J.; Majee, B. *J. Chem. Soc., Dalton Trans.* **1983**, 363. Vollano, J. F.; Day, R. O.; Rau, D. N.; Chandrasekhar, V.; Holmes, R. R. *Inorg. Chem.* **1984**, *23*, 3153. Senn, D. R.; Gladysz, J. A.; Emerson, K.; Larsen, R. D. *Inorg. Chem.* **1987**, *26*, 2739. Nakamura, E.; Kuwajima, I. *Chem. Lett.* **1983**, 59.

(14) Bancroft, G. M.; Davies, B. W.; Payne, N. C.; Sham, T. K. *J. Chem. Soc., Dalton Trans.* **1975**, 973.

Electron Transfer in DNA: Predictions of Exponential Growth and Decay of Coupling with Donor–Acceptor Distance

Steven M. Risser and David N. Beratan*

Department of Chemistry, University of Pittsburgh Pittsburgh, Pennsylvania 15260

Thomas J. Meade*

Beckman Institute, California Institute of Technology Pasadena, California 91125

Received November 19, 1992

Experimental and theoretical work indicates the importance of protein structure in controlling electron-transfer (ET) reactions.[1] Recently, great interest has been shown in exploring electronic coupling interactions in DNA. We report here that the electronic coupling calculated for a recently synthesized class of DNA oligomers with rigidly attached donors and acceptors[3] displays a remarkable dependence on the nucleic acid structure. Indeed, a reversal in the *sign* of the exponential decay parameter is found in some cases if the donor–acceptor couplings are fit to a single exponential expression. The sign reversal reflects the inadequacy of single exponential models for describing bridge-mediated electron-transfer reaction rates. These effects in DNA oligomers arise from the three-dimensional structure of the double helix. The couplings do decay monotonically with the tunneling pathway length[4] between donor and acceptor, *ơl* (estimated from tunneling pathway analysis), but not with the direct through-space donor–acceptor separation distance.

The rate of long-range electron transfer is proportional to the electron tunneling matrix element squared, $|T_{DA}|^2$. Within the Born–Oppenheimer and Franck–Condon approximations,[4,5] the matrix element can be written

$$T_{DA} = \sum_{ij} V_{Di} G_{ij} V_{jA}$$

where $V_{Di(jA)}$ is the coupling between the donor (acceptor) and bridge site i (j) and G_{ij} is the Green's function of the bridge. The matrix form of the Green's function at energy E is $(\mathbf{H} - E\mathbf{S})\mathbf{G} = \mathbf{S}$ where $\mathbf{H}$ is the bridge Hamiltonian and $\mathbf{S}$ is the overlap matrix.[4] We have used an extended-Hückel Hamiltonian (used successfully in prior studies of macromolecule ET[6]) to calculate the Green's function for double-stranded DNA oligomers up to eight units in length. From the elements of the Green's function, we calculate the component in the ribose 2′ carbon sp^3 orbital (C atom adjacent to the base pair connection), as this is the attachment site in specific redox-labeling studies.[3] This method of calculating T_{DA} has the advantage that it includes all multiple pathways and interference effects to all orders, so the accuracy of the coupling element is limited only by the choice of electronic Hamiltonian.

We have calculated the bridge contribution to $T_{DA}/(V_{D1}V_{NA}) = G_{1N}$ for a series of DNA oligomers of one to eight AT base pairs

(1) (a) *Structure and Bonding 75. Long range electron transfer in biology*; Springer Verlag: New York, 1991. (b) *Metal Ions in Biological Systems*; Sigel, H., Sigel, A., Eds.; Marcel Dekker Press: New York, 1991; Vol. 27.

(2) (a) Purugganan, M. D.; Kumar, C. V.; Turro, N. J.; Barton, J. K. *Science* **1988**, *241*, 1645. (b) Turro, N. J.; Barton, J. K.; Tomalia, D. A. *Acc. Chem. Res.* **1991**, *24*, 332. (c) Brun, A. M.; Harriman, A. *J. Am. Chem. Soc.* **1991**, *113*, 8153. (d) Orellana, G.; Kirschdemesmaeker, A.; Barton, J. K.; Turro, N. J. *Photochem. Photobiol.* **1991**, *499*, 54.

(3) Meade, T. J., submitted for publication.

(4) (a) Beratan, D. N.; Onuchic, J. N.; Winkler, J. R.; Gray, H. B. *Science* **1992**, *258*, 1740. (b) Onuchic, J. N.; Beratan, D. N.; Winkler, J. R.; Gray, H. B. *Annu. Rev. Biophys. Biomol. Struct.* **1992**, *21*, 349 and references therein.

(5) See Economou, E. N. *Green's Functions in Quantum Physics*; Springer Verlag: New York, 1990.

(6) (a) Siddarth, P.; Marcus, R. A. *J. Phys. Chem.* **1992**, *96*, 3213. (b) Broo, A.; Larsson, S. *J. Phys. Chem.* **1991**, *95*, 4925. (c) Christensen, H. E. M.; Conrad, L. S.; Mikkelsen, K. V.; Nielsen, M. K.; Ulstrup, J. *Inorg. Chem.* **1990**, *29*, 2808.

0002-7863/93/1515-2508$04.00/0

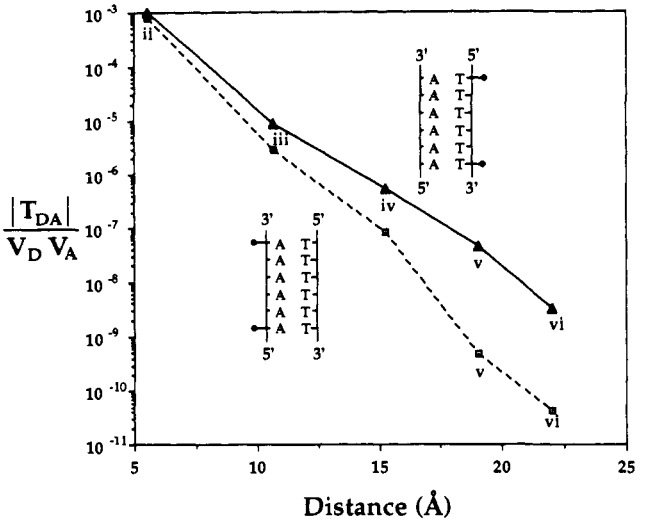

Figure 1. Coupling along each ribose phosphate backbone strand (3′–5′ couplings) of the duplex oligo(AT). The structures show the geometrical relationship between the groups with which the donor and acceptor interact.

and report the coupling between the ribose 2′ carbon sp^3 orbitals.[7] In Figure 1 we show the coupling between the 3′ and 5′ chain-end ribose ring 2′ carbons of the same ribose phosphate strand for oligo(AT). The coupling along either the A or the T strands shows a monotonic decrease with distance and number of base pairs, with somewhat different decay rates. This is not the case when we calculate the coupling between the two 3′ ends of the DNA oligomer (Figure 2). The coupling between the two 3′ ends decreases by 2 orders of magnitude as the oligomer increases from two to four base pairs, despite a 0.5-Å *decrease* in donor–acceptor distance.[7] In spite of the shrinking direct (or through-space) donor–acceptor distance between 3′ chain ends as the oligomer grows, there is a developing minor groove in the intervening space. Thus, efficient direct pathways for donor–acceptor coupling do not exist. This is not the case for the 5′-to-5′ couplings, which decrease monotonically with both the distance and the number of base pairs. The same qualitative behavior in the distance dependence of the coupling is seen for the experimentally relevant sequence UGCATCGA (Figure 2b). This sequence was recently synthesized and labeled with covalently attached transition-metal donor and acceptor groups.[3] Comparison of Figures 1 and 2 shows that coupling along a single ribose phosphate strand is larger than for the cross-strand coupling in a given number of base pairs, even though the coupling distance is larger along the strand. Also, the double helix symmetry makes the 3′–3′ and 5′–5′ coupling strengths slightly different in poly(AT) and poly(TA), although the qualitative behavior is similar. We have also estimated electronic couplings on the basis of the tunneling pathway model that was developed for protein electron-transfer reactions.[8] The trends in the results reported here agree with those of the tunneling pathways analysis for these molecules, including the anomalously small coupling in the 3′–3′ oligomers arising from the position of the minor groove. Studies are underway to determine whether or not solvent molecules in the minor groove provide efficient tunneling pathways. Indeed, the double helix is an excellent system in which to study the interplay between covalent bond and solvent-mediated pathways. Additional studies will show the extent to which deviations of DNA geometries from the idealized ones used here alter the predicted trends in the long-range electronic couplings.

T_{DA} is sensitive to the average orbital energies of the donor and acceptor states that are oxidized/reduced.[9] Although the present

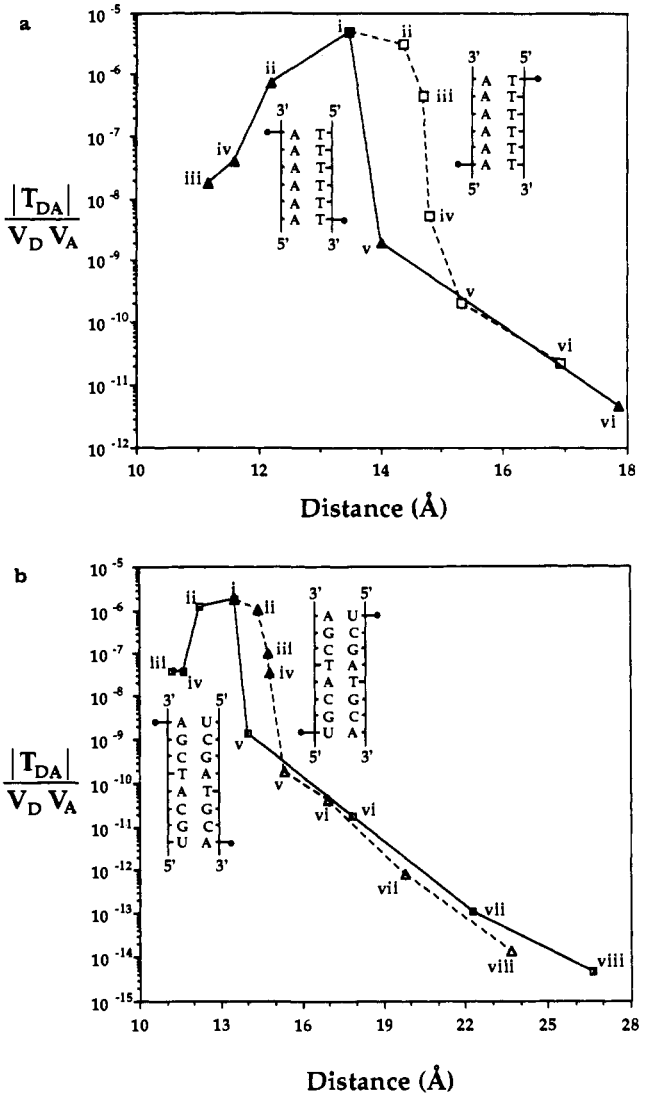

Figure 2. (a) Calculated couplings between the 3′–3′ (solid) and 5′–5′ (dashed) ribose rings (atom 2′) in duplex oligo(AT) vs donor–acceptor distance. Note that over the distance range from 11–13.5 Å the coupling grows with increasing donor–acceptor separation distance. (b) Calculated couplings between the 3′–3′ and 5′–5′ ribose rings (atom 2′) in duplex UGCATCGA vs donor–acceptor distance.

results were calculated for a tunneling energy near the middle of the π–π^* gap of the AT monomer, the qualitative mediation effects discussed above were found to be insensitive to the precise tunneling energy chosen. Calculations of coupling across a base pair with a variable number of neighboring pairs showed that the DNA-mediated coupling across a single base pair is almost unchanged as the neighbors are added. This suggests that the results we report for T_{DA} as a function of the spatial relationship between donor and acceptor should obtain if the "oligomer" is imbedded in a longer strand of DNA.

Tunneling phenomena are expected to be exquisitely sensitive to the chemistry of the barrier. We find that in homo(AT) oligomers of a given length the coupling between ribose rings may differ by several orders of magnitude. For small oligomers, the exponential constants describing the average change in coupling with distance may even be *positive* over a limited distance range for species at a particular geometry. Work is in progress to calculate the coupling between intercalated donor–acceptor species and for a variety of base pair sequences. The results of this study suggest that electron-transfer rates in DNA will be diagnostic of the donor and acceptor binding sites and base pair composition. Electron-transfer rates measured on a series of ruthenium-modified

(7) Structures were built with standard DNA bond lengths and angles using BIOGRAF (Molecular Simulations Inc.).

(8) (a) Onuchic, J. N.; Beratan, D. N. *J. Chem. Phys.* **1990**, *92*, 722. (b) Beratan, D. N.; Betts, J. N.; Onuchic, J. N. *Science* **1991**, *252*, 1285.

(9) Beratan, D. N.; Hopfield, J. J. *J. Am. Chem. Soc.* **1984**, *106*, 1584.

duplexes will provide crucial tests of these predictions.[3]

Acknowledgment. Support of this research by the Department of Energy's Advanced Industrial Concepts Division (D.N.B.), a National Science Foundation National Young Investigator Award (D.N.B.), and an award from Research Corporation (T.J.M.) is gratefully acknowledged. We also thank the Biological Imaging Center of the Beckman Institute, California Institute of Technology, for generous support.

Boron Atom Reactions with Acetylene. Ab Initio Calculated and Observed Isotopic Infrared Spectra of the Borirene Radical BC_2H_2. A Fingerprint Match

Jan M. L. Martin† and Peter R. Taylor

San Diego Supercomputer Center
P.O. Box 85608
San Diego, California 92186-9784

Parviz Hassanzadeh‡ and Lester Andrews*

Department of Chemistry
University of Virginia
Charlottesville, Virginia 22901
Received December 4, 1992

Boron atom reactions with small molecules such as O_2, H_2O, N_2, CO, and CH_4 have produced new boron species for matrix infrared spectroscopic characterization.[1-7] The boron–acetylene reaction is of particular interest because theoretical calculations suggest that both C—H insertion and C=C addition reactions will proceed readily.[8] The addition product borirene radical BC_2H_2 is expected to be a novel 2π-electron aromatic system like that predicted for borirene (HBC_2H_2)[9-11] and observed for substituted borirene species.[12,13] The infrared spectrum and MP2/DZP calculations on the borirene radical will be presented here.

Mixtures of argon/acetylene (200:1 to 800:1) were codeposited at 12 ± 1 K with laser-evaporated boron atoms [^{n}B: 80% ^{11}B, 20% ^{10}B and ^{10}B: 94% ^{10}B, 6% ^{11}B] using 40 mJ/pulse at the target as described previously.[1,3] Spectra for reaction of each boron sample with C_2H_2, $^{13}C_2H_2$, and C_2D_2 were collected at 0.5-cm^{-1} resolution. Samples were also subjected to UV photolysis and to annealing cycles, and more spectra were recorded.

Two spectral regions are of interest: the 2100–1900-cm^{-1} region shows three species with strong C=C stretching modes, which will be the subject of a full paper, and the 1200–1100-cm^{-1} region reveals two sharp product absorptions at 1175.3 and 1170.6 cm^{-1}

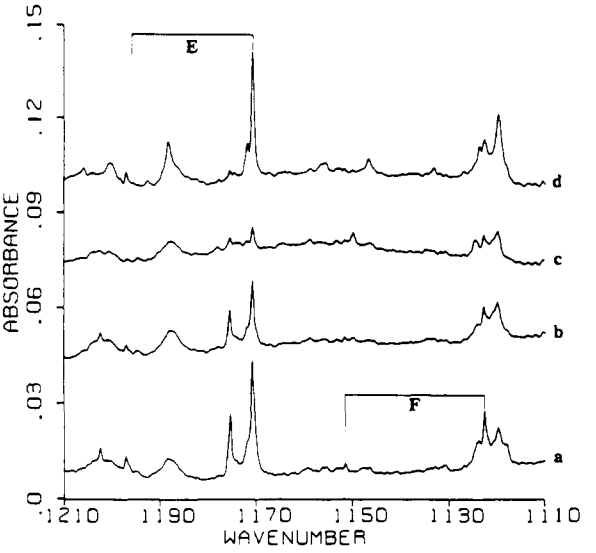

Figure 1. Infrared spectra in the 1210–1110-cm^{-1} region for natural isotopic boron atoms and 400:1 Ar/C_2H_2 sample at 12 ± 1 K: (a) spectrum after 5-h codeposition; (b) spectrum after $\lambda > 290$ nm photolysis for 45 min; (c) spectrum after $\lambda > 254$ nm photolysis for 45 min; and (d) spectrum after annealing to 28 ± 1 K.

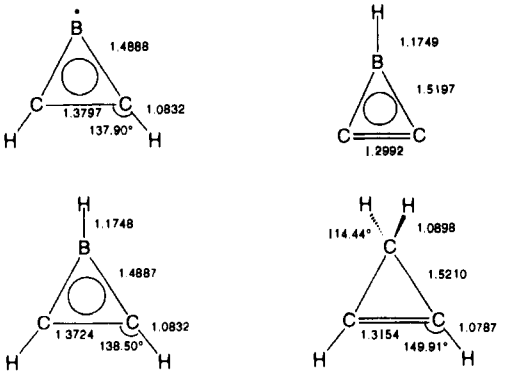

Figure 2. MP2/DZP optimized geometries (Å, deg) for the C_{2v} molecules HBC_2, BC_2H_2, HBC_2H_2, and C_3H_4.

(E) and 1122.7 cm^{-1} (F), which will be considered here. Figure 1a shows the latter absorptions after codeposition for 5 h. The E doublet and F band are decreased 40% by $\lambda > 290$ nm photolysis, Figure 1b. Further $\lambda > 254$ nm irradiation almost destroyed the E and F bands, Figure 1c. Annealing to 18 ± 1 K to allow diffusion and reaction of trapped boron atoms restored some of the 1170.6-cm^{-1} band, and acetylene absorptions did not change (not shown). Further annealing to 28 ± 1 K reproduced the 1170.6-cm^{-1} E band, but not the 1175.3-cm^{-1} band presumed to be a less stable matrix site, sharpened the F band, increased a 1119-cm^{-1} shoulder absorption, Figure 1d, and increased acetylene cluster absorptions. The 1188-cm^{-1} band that also increased on annealing is probably due to species E perturbed by C_2H_2.

Isotopic data for the E bands are given in Table I. The 1170.6-cm^{-1} band exhibits 26.4-cm^{-1} boron-10, 22.9-cm^{-1} carbon-13, and 1.2-cm^{-1} deuterium shifts and as such defines a symmetric B–C_2 stretching vibration. The natural boron isotopic 4:1 doublet demonstrates the presence of a single boron atom, and the observation of a single carbon-12,13 peak in a carbon-13 enriched sampled characterizes two equivalent carbon atoms. Species E thus contains one B, two equivalent C atoms, and hydrogen.

Calculations were done at the MP2 level[14] with the DZP (double-ζ plus polarization) basis set[15] using the GAUSSIAN 92

†On leave from Limburgs Universitair Centrum, Department SBG, Universitaire Campus, B-3590 Diepenbeek, Belgium, and University of Antwerp (UIA), Department of Chemistry, Institute for Materials Science, Universiteitsplein 1, B-2610 Wilrijk, Belgium.

‡Present address: Department of Chemistry, College of Sciences, Shiraz University, Shiraz, Iran.

(1) Burkholder, T. R.; Andrews. L. *J. Chem. Phys.* **1991**, *95*, 8697.
(2) Andrews, L.; Burkholder, T. R. *J. Phys. Chem.* **1991**, *95*, 8554.
(3) Hassanzadeh, P.; Andrews, L. *J. Phys. Chem.* **1992**, *96*, 9177.
(4) Hamrick, Y. M.; Van Zee, R. J.; Godbout, J. T.; Weltner, W., Jr.; Lauderdale, W. J.; Stanton, J. F.; Bartlett, R. J. *J. Phys. Chem.* **1991**, *95*, 2840, 5366.
(5) Burkholder, T. R.; Andrews, L. *J. Phys. Chem.* **1992**, *96*, 10195.
(6) Jeong, G. H.; Boucher, R.; Klabunde, K. J. *J. Am. Chem. Soc.* **1991**, *112*, 3332.
(7) Hassanzadeh, P.; Andrews, L. *J. Am. Chem. Soc.* **1992**, *114*, 9239.
(8) Flores, J. R.; Largo, A. *J. Phys. Chem.* **1992**, *96*, 3015.
(9) Krogh-Jespersen, K.; Cremer, D.; Dill, J. D.; Pople, J. A.; Schleyer, P. v. R. *J. Am. Chem. Soc.* **1981**, *103*, 2539.
(10) Budzelaar, P. H. M.; van der Kerk, S. M.; Krogh-Jespersen, K.; Schleyer, P. v. R. *J. Am. Chem. Soc.* **1986**, *108*, 3960.
(11) Byun, Y.-G.; Saebo, S.; Pittman, C. U. *J. Am. Chem. Soc.* **1991**, *113*, 3689.
(12) Eisch, J. J.; Shafii, B.; Rheingold, A. L. *J. Am. Chem. Soc.* **1987**, *109*, 2526.
(13) Eisch, J. J.; Shafii, B.; Odom, J. D.; Rheingold, A. L. *J. Am. Chem. Soc.* **1990**, *112*, 1847.
(14) Møller, C.; Plesset, M. S. *Phys. Rev.* **1934**, *46*, 618. Binkley, J. S.; Pople, J. A. *Int. J. Quantum Chem.* **1975**, *9*, 229.

0002-7863/93/1515-2510$04.00/0